

# Microscopic study of $^{40}\text{Ca}+^{58,64}\text{Ni}$ fusion reactions

D. Bourgin<sup>1,2,\*</sup>, C. Simenel<sup>3</sup>, S. Courtin<sup>1,2,4</sup>, and F. Haas<sup>1,2</sup>

<sup>1</sup>*IPHC, Université de Strasbourg, F-67037 Strasbourg, France*

<sup>2</sup>*CNRS, UMR7178, F-67037 Strasbourg, France*

<sup>3</sup>*Department of Nuclear Physics, RSPE, Australian National University, Canberra, Australian Capital Territory 0200, Australia and*

<sup>4</sup>*USIAS, F-67083 Strasbourg, France*

(Dated: March 7, 2022)

**Background:** Heavy-ion fusion reactions at energies near the Coulomb barrier are influenced by couplings between the relative motion and nuclear intrinsic degrees of freedom of the colliding nuclei. The time-dependent Hartree-Fock (TDHF) theory, incorporating the couplings at the mean-field level, as well as the coupled-channels (CC) method are standard approaches to describe low energy nuclear reactions.

**Purpose:** To investigate the effect of couplings to inelastic and transfer channels on the fusion cross sections for the reactions  $^{40}\text{Ca}+^{58}\text{Ni}$  and  $^{40}\text{Ca}+^{64}\text{Ni}$ .

**Methods:** Fusion cross sections around and below the Coulomb barrier have been obtained from coupled-channels (CC) calculations, using the bare nucleus-nucleus potential calculated with the frozen Hartree-Fock method and coupling parameters taken from known nuclear structure data. The fusion thresholds and neutron transfer probabilities have been calculated with the TDHF method.

**Results:** For  $^{40}\text{Ca}+^{58}\text{Ni}$ , the TDHF fusion threshold is in agreement with the most probable barrier obtained in the CC calculations including the couplings to the low-lying octupole  $3_1^-$  state for  $^{40}\text{Ca}$  and to the low-lying quadrupole  $2_1^+$  state for  $^{58}\text{Ni}$ . This indicates that the octupole and quadrupole states are the dominant excitations while neutron transfer is shown to be weak. For  $^{40}\text{Ca}+^{64}\text{Ni}$ , the TDHF barrier is lower than predicted by the CC calculations including the same inelastic couplings as those for  $^{40}\text{Ca}+^{58}\text{Ni}$ . TDHF calculations show large neutron transfer probabilities in  $^{40}\text{Ca}+^{64}\text{Ni}$  which could result in a lowering of the fusion threshold.

**Conclusions:** Inelastic channels play an important role in  $^{40}\text{Ca}+^{58}\text{Ni}$  and  $^{40}\text{Ca}+^{64}\text{Ni}$  reactions. The role of neutron transfer channels has been highlighted in  $^{40}\text{Ca}+^{64}\text{Ni}$ .

PACS numbers: 25.70.Jj, 24.10.Eq, 21.60.Jz

## I. INTRODUCTION

Heavy-ion fusion cross sections near the Coulomb barrier are influenced by couplings of the relative motion to nuclear shape deformations and vibrations [1–3]. The effects of these couplings can be investigated by coupled-channels (CC) calculations [4–11] and time-dependent Hartree-Fock (TDHF) calculations [12–14].

Nucleon transfer channels have also been shown to affect the fusion process [15–19]. However, a deep understanding of the interplay between fusion and transfer is still needed. This is partly due to the difficulty to construct predictive theoretical models of fusion incorporating the dissipation and Q-value effects of transfer. Transfer channels are indeed incorporated within CC models in a simplified fashion [20]. In addition, recent progresses of microscopic description of transfer reactions are mostly limited to the mean-field approximation [21–25], to small [26–28] and semi-classical [29–31] fluctuations. Nevertheless, comparison between experimental data and theoretical calculations of fusion properties such as barriers and cross sections is expected to shed light on the importance of coupling to transfer channels.

On the one hand, CC calculations treat the couplings to inelastic channels in a fully quantum mechanical approach. However, they require input parameters for the nuclear potential as well as coupling parameters of collective states in the colliding nuclei. The TDHF approach, on the other hand, often uses Skyrme energy density functionals [32] which are fitted on basic nuclear structure properties [33] as a unique input. It also naturally incorporates both coupling to inelastic and transfer channels. However, these couplings are only treated at the mean-field level. A new approach has been proposed to combine these two complementary theories in Ref. [14]. Other works have also incorporated microscopic ingredients in CC calculations [11].

Recently, the fusion excitation functions of  $^{40}\text{Ca}+^{58}\text{Ni}$  and  $^{40}\text{Ca}+^{64}\text{Ni}$  [34] have been measured at energies around and below the Coulomb barrier to study the influence of the projectile and target nuclear structures on the fusion process. CC calculations were performed with the CCFULL code [35], using the Akyüz-Winther nuclear potential [36, 37] and including the most relevant inelastic channels, i.e. the octupole-phonon excitation ( $0_{\text{gs}}^+ \rightarrow 3_1^-$ ) for  $^{40}\text{Ca}$  and the quadrupole-phonon excitation ( $0_{\text{gs}}^+ \rightarrow 2_1^+$ ) for both  $^{58}\text{Ni}$  and  $^{64}\text{Ni}$ . The effect of the positive  $Q$  value two-neutron transfer channel in  $^{40}\text{Ca}+^{64}\text{Ni}$  was also schematically taken into account. The  $^{40}\text{Ca}+^{64}\text{Ni}$  system has positive nucleon

\* dominique.bourgin@iphc.cnrs.fr

transfer  $Q$  values, whereas  $^{40}\text{Ca}+^{58}\text{Ni}$  has only negative nucleon transfer  $Q$  values. The fusion cross sections for  $^{40}\text{Ca}+^{58}\text{Ni}$  are well reproduced at sub-barrier energies by including couplings to inelastic channels in the CC calculations. For  $^{40}\text{Ca}+^{64}\text{Ni}$ , the fusion cross sections are underestimated by including only couplings to inelastic channels. The additional coupling to the two-neutron transfer channel turned out to be essential to describe the large fusion cross sections at sub-barrier energies for this system [34].

In this work, we have analysed the two fusion reactions  $^{40}\text{Ca}+^{58}\text{Ni}$  and  $^{40}\text{Ca}+^{64}\text{Ni}$  with microscopic calculations, employing the Skyrme-functional SLy4d [38]. The method is described in Sec. II. Results of the calculations are presented in Sec. III and compared with experimental data. In Sec. IV, we summarize our conclusions.

## II. THEORETICAL APPROACH

The time-dependent Hartree-Fock (TDHF) theory is a mean-field approximation of the many-body dynamics. It was initially proposed by Dirac [39] to describe electrons in atoms, in which case the particles interact via the Coulomb interaction. Direct computation of the Hartree-Fock mean-field in nuclei remains a problem as the interaction between nucleons in the nuclear medium is still unknown. However, the development of phenomenological Skyrme effective interactions [32] allowed to bypass the problem by using the resulting energy density functional (instead of the nucleon-nucleon interaction) to express the mean-field potential [33].

Many parameterisations of the Skyrme functional have been developed over the past. However, most of the Skyrme parameterisations have been fitted assuming a one-body center-of-mass correction to describe the nuclei in their intrinsic frame. This is implemented by replacing the nucleon mass  $m$  with  $Am/(A-1)$ , where  $A$  is the number of nucleons. Although this usually improves the structure of light nuclei, such correction should not be applied when studying collisions as it induces a spurious dependence on the initial number of nucleons of the collision partners. Therefore, we use the SLy4d parameterisation [38] which has been derived without center-of-mass correction. Note that other recent parameterisations have been derived without this correction, such as the Quark-Meson Coupling 700 [40] and the Universal Nuclear Energy Density Functional [41] parameterisations. Comparison with these interactions will be the subject of a future work.

The TDHF approach has become a standard tool to describe nuclear reactions (see Refs. [42, 43] for a review). This has been made possible thanks to calculations in three dimensions including spin-orbit interaction [38, 44–48]. In particular, TDHF predictions of barriers and fusion cross sections are in good agreement with

experimental data [12–14, 21, 49, 50]. Importantly, it incorporates dynamical effects such as vibration [45, 51] and particle transfer [22, 23, 28] which are crucial at near barrier energies [12, 50].

An important drawback of mean-field calculations, however, is the impossibility to describe tunneling of the many-body wave function. As a result, sub-barrier fusion cannot be directly investigated in TDHF. Nevertheless, TDHF codes can be used to compute fusion thresholds including dynamical effects [12, 21, 50, 52–54].

To estimate sub-barrier fusion cross sections, one has to determine a nucleus-nucleus potential and to compute the sub-barrier transmission with a barrier penetration model. Microscopic potentials can be calculated directly from TDHF dynamics [12, 55]. Alternatively, one can start with the bare potential computed from a frozen Hartree-Fock approach [12, 21] and use a CC code to incorporate the dynamical couplings to collective modes following the approach proposed in Ref. [14]. The properties of the collective phonons are either known experimentally or computed theoretically, for instance in the linear response theory with a TDHF code [46–48, 56–60]. Therefore, the approach of Ref. [14] allows to use the same Skyrme functional to compute both the bare potential and the deformation parameters of the collective excited states.

In the present work, we follow the approach of Ref. [14] to extract various information on the fusion dynamics:

- The bare potential is computed with the Frozen Hartree-Fock approach.
- Fusion cross sections incorporating couplings to low-lying vibrational states are computed with the CC approach using the CCFULL code [35] with the above potential and experimental properties of low-lying vibrational states (energy and deformation parameters).
- The resulting barrier distributions are compared with fusion thresholds computed directly from TDHF, and incorporating dynamical effects at the mean-field level, such as couplings to vibrational states and to transfer channels.
- The importance of transfer channels is estimated with near-barrier TDHF calculations of transfer probabilities using the particle number projection technique developed in Ref. [23].

Combining these information for  $^{40}\text{Ca}+^{58,64}\text{Ni}$  reactions and comparing with experimental data will then allow to identify the impact of transfer mechanisms on fusion in these reactions.

The HF and TDHF calculations are performed with the EV8 [61] and TDHF3D [38] codes, respectively. The SLy4d interaction [38] is used. Unless specified, pairing is included in static calculations at the BCS level and single-particle occupation numbers are kept constant during the dynamics. The surface pairing interaction is

used [62]. All calculations are performed with a mesh space of 0.8 fm and a time step of  $1.5 \times 10^{-24}$  s.

In our calculations, all nuclei are spherical, except for  $^{64}\text{Ni}$  which exhibits a very small triaxial quadrupole deformation with a maximum quadrupole moment of 1.0 fm<sup>2</sup>. We thus treat it as spherical. Note that other functionals could result in slightly deformed ground-states [63–66].

### III. RESULTS

#### A. Fusion excitation functions

The frozen Hartree-Fock potential is computed from the HF ground-state one-body density matrices  $\rho_{1,2}$  of the two colliding nuclei at a distance  $R$  between their centers of mass. The total energy  $E[\rho_1 + \rho_2](R)$  of the system is given by the energy density functional including Coulomb energy. The nucleus-nucleus potential is then obtained by removing the HF energy of the ground-states  $V(R) = E[\rho_1 + \rho_2](R) - E_{\text{HF}}[\rho_1] - E_{\text{HF}}[\rho_2]$ .

The resulting bare potential barrier radii  $R_b$  and heights  $V_b$  are listed in Table I. As expected, the bare potential barrier radius is larger, and the height smaller, for  $^{40}\text{Ca} + ^{64}\text{Ni}$  than for  $^{40}\text{Ca} + ^{58}\text{Ni}$  due to the larger size of  $^{64}\text{Ni}$ . As a comparison, the bare potential barriers calculated from the frozen HF method and from the Bass model [67] are reported in Fig. 3. The frozen HF method predicts barriers which are noticeably smaller than the more phenomenological parameterisation by Bass.

TABLE I. Bare potential barrier characteristics from the frozen HF method and from the Bass model [67] as well as TDHF fusion thresholds for  $^{40}\text{Ca} + ^{58,64}\text{Ni}$ .

Barrier characteristics	$^{40}\text{Ca} + ^{58}\text{Ni}$	$^{40}\text{Ca} + ^{64}\text{Ni}$
$V_b^{\text{frozen}}$ [MeV]	74.15	72.26
$R_b^{\text{frozen}}$ [fm]	10.11	10.40
$V_b^{\text{Bass}}$ [MeV]	75.73	74.66
$R_b^{\text{Bass}}$ [fm]	10.65	10.80
$V_b^{\text{TDHF}}$ [MeV]	71.70	69.06

A Saxon-Woods parameterisation of the nuclear potential was extracted from the frozen potential to be used in CC calculations. The potential well depths  $V_0$ , nuclear radii  $r_0$  and surface diffuseness  $a$  parameters are listed in Table II. The resulting fusion cross sections  $\sigma_f$  were computed with the CCFULL code and are plotted with dashed-lines in Fig. 1. The experimental data are taken from Ref. [34]. For the two studied systems, the CC calculations with no couplings to inelastic and transfer channels underestimate the measured fusion cross sections at sub-barrier energies by about two orders of magnitude.

The intensity of the couplings to low-lying vibrations is determined by the energy and deformation parameter of the phonons. The latter can be obtained from nuclear structure experimental data or theoretical calculations.

TABLE II. Saxon-Woods parameterisation of the nuclear potential extracted from the frozen potential for  $^{40}\text{Ca} + ^{58,64}\text{Ni}$ .

System	$V_0$ [MeV]	$r_0$ [fm]	$a$ [fm]
$^{40}\text{Ca} + ^{58}\text{Ni}$	87.16	1.16	0.62
$^{40}\text{Ca} + ^{64}\text{Ni}$	106.12	1.15	0.64

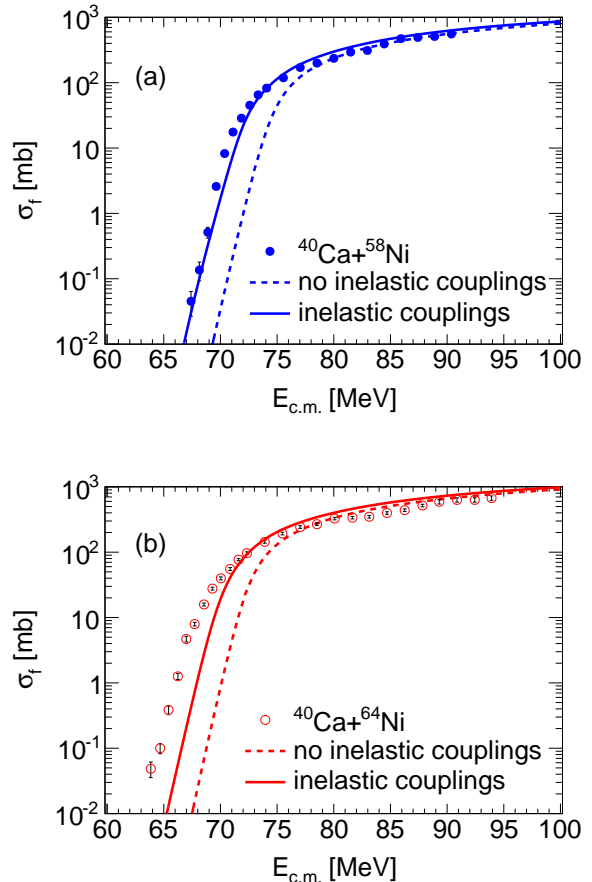


FIG. 1. (Color online) Experimental and calculated fusion excitation functions for  $^{40}\text{Ca} + ^{58}\text{Ni}$  (a) and  $^{40}\text{Ca} + ^{64}\text{Ni}$  (b). The coupled-channels calculations were performed with the frozen HF potential and the coupling parameters of the low-lying octupole state for  $^{40}\text{Ca}$  and of the low-lying quadrupole states for  $^{58,64}\text{Ni}$  given in Table III.

For the present systems, the main effect is expected from the coupling to low-lying octupole modes in  $^{40}\text{Ca}$  and quadrupole modes in  $^{58,64}\text{Ni}$  [68, 69]. The energy and deformation parameters of the associated first phonons are experimentally well known for these isotopes and are summarised in Table III.

Coupled-channel calculations have been performed including couplings to the low-lying  $2_1^+$  and  $3_1^-$  states with the CCFULL code [35]. The resulting fusion cross sections are shown with solid lines in Fig. 1. For  $^{40}\text{Ca} + ^{58}\text{Ni}$ , the measured fusion cross sections are well reproduced

TABLE III. Excitation energies ( $E$ ) as well as quadrupole and octupole deformation parameters ( $\beta_{2,3}$ ) of the low-lying vibrational states included in the CC calculations. For references, see the caption of Table I in Ref. [34].

Nucleus	$J^\pi$	$E$ [keV]	$\beta_{2,3}$
$^{40}\text{Ca}$	$3_1^-$	3736	0.40
$^{58}\text{Ni}$	$2_1^+$	1454	0.18
$^{64}\text{Ni}$	$2_1^+$	1346	0.16

over the energy range, especially at sub-barrier energies where the fusion process occurs by quantum tunneling. The couplings to the  $3_1^-$  state for  $^{40}\text{Ca}$  and  $2_1^+$  state for  $^{58}\text{Ni}$  explain the enhancement of the fusion cross sections in this energy range.

For  $^{40}\text{Ca}+^{64}\text{Ni}$ , the CC calculations with couplings to inelastic channels still underestimate the measured fusion cross sections at sub-barrier energies. These couplings are the same as those for  $^{40}\text{Ca}+^{58}\text{Ni}$  since  $^{58}\text{Ni}$  and  $^{64}\text{Ni}$  have similar nuclear properties. Similar results were obtained in Ref. [34], using the Akyüz-Winther nuclear potential and including the same inelastic couplings. However, the diffuseness parameter of the Akyüz-Winther nuclear potential was slightly increased for  $^{40}\text{Ca}+^{64}\text{Ni}$  to fit the fusion cross sections around the Coulomb barrier, whereas the only input parameters in the frozen Hartree-Fock method are those of the Skyrme energy density functional.

Couplings to nucleon transfer channels could also play an important role in the fusion process [19]. The  $^{40}\text{Ca}+^{64}\text{Ni}$  fusion reaction has positive  $Q$  values for the transfer of neutrons from  $^{64}\text{Ni}$  to  $^{40}\text{Ca}$  (neutron pick-up) and protons from  $^{40}\text{Ca}$  to  $^{64}\text{Ni}$  (proton stripping), whereas  $^{40}\text{Ca}+^{58}\text{Ni}$  has only negative nucleon transfer  $Q$  values. Corresponding  $Q$  values are listed in Table IV. The importance of neutron transfer in  $^{40}\text{Ca}+^{64}\text{Ni}$  will be confirmed with TDHF calculations in section III C.

TABLE IV. Corrected- $Q$  values in MeV of transfer reactions for  $^{40}\text{Ca}+^{58,64}\text{Ni}$  ( $Q_{\text{corr}} = Q_{\text{tr}} + V_b^{\text{in}} - V_b^{\text{out}}$ ) [70]. The indicated + sign corresponds to neutron pick-up and the - sign to proton stripping.

System	+1n	+2n	+3n	-1p	-2p	-3p
$^{40}\text{Ca}+^{58}\text{Ni}$	-3.80	-2.52	-11.19	-3.75	-3.60	-11.95
$^{40}\text{Ca}+^{64}\text{Ni}$	-1.23	3.47	0.86	0.26	4.19	0.88

### B. TDHF fusion thresholds and experimental fusion barrier distributions

Based on a deterministic mean-field approximation, the TDHF theory can only give fusion probabilities which are either 0 or 1 for a given initial energy and impact parameter [49], and for an initial orientation in case of

deformed nuclei [52]. As a result, it can be used to compute fusion thresholds including dynamical effects due to internal excitations, deformation to all orders, neck formation and nucleon exchange.

Examples of time evolutions of the distance between the colliding nuclei in  $^{40}\text{Ca}+^{58,64}\text{Ni}$  are plotted in Fig. 2. This distance is defined as the distance between the centres of masses computed on each side of the neck. The energies are chosen to be just above and below the fusion threshold with a difference of only 50 keV.

Interestingly, both systems exhibit similar behaviours. In particular, the fragments are in contact during  $\sim 1$  zs ( $10^{-21}$  s) before fusion is decided. Similar times were obtained for near barrier collisions in lighter [38, 71] and similar [14, 28] mass regions. These times are relatively short in comparison with heavier systems computed with TDHF where typical contact times of few zeptoseconds [72] or more in case of quasi-fission reactions [43, 53, 73–75] are often obtained, leading to possible large mass transfer [76, 77]. Nevertheless, contact times of  $\sim 1$  zs are long enough to allow transfer of one or more nucleons [23, 30, 31, 78], in particular in the case of positive  $Q$  value reactions as will be seen in section III C.

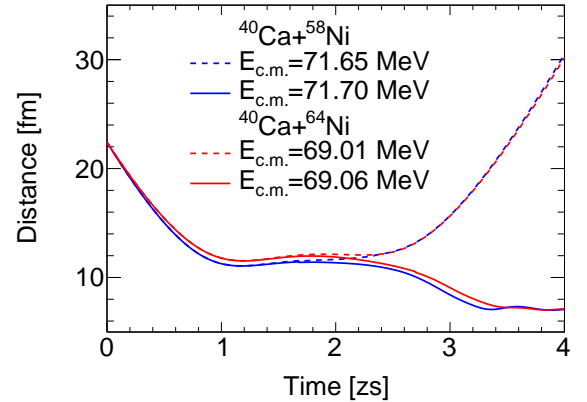


FIG. 2. (Color online) Time evolutions of the distance between the colliding nuclei in  $^{40}\text{Ca}+^{58,64}\text{Ni}$  just above (solid lines) and below (dashed lines) the fusion threshold.

The resulting fusion thresholds are listed in Table I. These thresholds are lower than the bare potential barrier heights computed with the frozen HF method (2.45 MeV for  $^{40}\text{Ca}+^{58}\text{Ni}$  and 3.20 MeV for  $^{40}\text{Ca}+^{64}\text{Ni}$ ). This lowering of the fusion barrier height is induced by dynamical effects such as couplings to inelastic and nucleon transfer channels. These couplings are also responsible for the enhancement of sub-barrier fusion cross sections with respect to the uncoupled case (see Fig. 1).

The fusion and bare potential barrier heights can be compared to the centroids of the measured and calculated barrier distributions which are plotted in Fig. 3. These barrier distributions [79] were derived from the second derivative of ( $E_{c.m.} \times \sigma_f$ ) with respect to  $E_{c.m.}$ , using the



three-point difference formula [2], with an energy step of  $\Delta E_{c.m.} \simeq 1.5$  MeV below the Coulomb barrier and 3 MeV above the Coulomb barrier.

We see in Fig. 3 that the TDHF fusion threshold for  $^{40}\text{Ca}+^{58}\text{Ni}$  is in good agreement with the large structure of the measured barrier distribution as well as the maximum of the CC barrier distribution (solid line). As the TDHF result includes all type of couplings, this indicates that most of the lowering of the fusion threshold is accounted for by the coupling to the  $3_1^-$  state in  $^{40}\text{Ca}$  and to the  $2_1^+$  state in  $^{58}\text{Ni}$ .

For  $^{40}\text{Ca}+^{64}\text{Ni}$ , the TDHF barrier is also in agreement with the large structure of the measured barrier distribution but it is lower than the maximum of the CC barrier distribution (solid line). This indicates that the couplings to transfer channels, which are included in TDHF dynamics but not in the CC calculations, could play a role in the lowering of the fusion threshold.

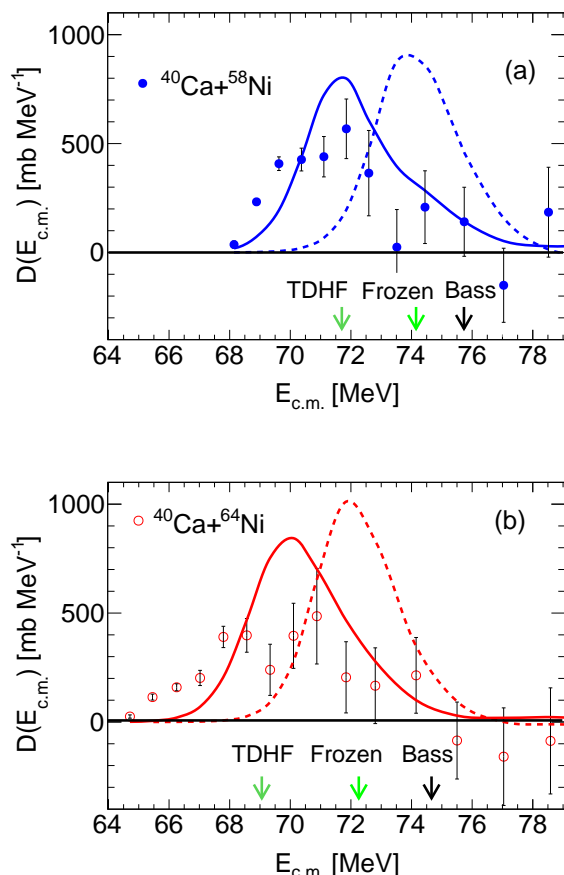


FIG. 3. (Color online) Experimental and calculated barrier distributions for  $^{40}\text{Ca}+^{58}\text{Ni}$  (a) and  $^{40}\text{Ca}+^{64}\text{Ni}$  (b). The coupled-channels calculations were performed with the CC-FULL code, using the frozen potential and the coupling parameters of the low-lying octupole state for  $^{40}\text{Ca}$  and of the low-lying quadrupole states for  $^{58,64}\text{Ni}$  given in Table III. The Bass, frozen HF and TDHF barriers are shown with arrows on the  $E_{c.m.}$ -axis.

### C. Sub-barrier transfer probabilities

Neutron transfer probabilities were computed using the particle number projection technique developed in Ref. [23]. For simplicity, these calculations were performed without pairing correlations. This is sufficient to provide a reasonable estimate of the overall importance of transfer. More predictive transfer probabilities for individual transfer channels would require the inclusion of dynamical pairing correlations [80, 81].

Neutron number distributions of the Ca projectile-like fragment in the exit channel were calculated at  $E_{c.m.} = 71.65$  MeV for  $^{40}\text{Ca}+^{58}\text{Ni}$  and at  $E_{c.m.} = 69.01$  MeV for  $^{40}\text{Ca}+^{64}\text{Ni}$ . These energies are located just below the TDHF fusion thresholds.

As can be seen in Fig. 4, the sum of the transfer probabilities does not exceed 0.04 in  $^{40}\text{Ca}+^{58}\text{Ni}$  near barrier collisions. This confirms our previous conclusion that the impact of transfer channels on fusion is small in this reaction. This was expected due to negative  $Q$  values for transfer reactions in this system.

Transfer probabilities are much larger in the  $^{40}\text{Ca}+^{64}\text{Ni}$  system, with a total transfer probability of  $\sim 0.7$ . In this case, the dominant channel is the transfer of one neutron from  $^{64}\text{Ni}$  to  $^{40}\text{Ca}$ , followed by the two-neutron transfer channel. However, the relative weighting between individual channels could be strongly modified with the inclusion of dynamical pairing [81] favouring pair transfer channels [82, 83].

Quantitatively, the couplings to the vibrational states accounts for a lowering of the barrier by  $\sim 2$  MeV in  $^{40}\text{Ca}+^{64}\text{Ni}$ , while TDHF calculations predicts that the fusion thresholds should be lowered by more than 3 MeV. It is likely that the transfer channels are responsible for this difference. Indeed, they could easily affect the fusion process by, e.g., facilitating the formation of a neck between the fragments.

## IV. SUMMARY

Microscopic and coupled-channel calculations have been performed for the  $^{40}\text{Ca}+^{58,64}\text{Ni}$  reactions near the fusion barrier. The only input parameters are those of the Skyrme energy density functional. Fusion cross sections around and below the Coulomb barrier were obtained from CC calculations, using the bare nucleus-nucleus potential computed with the frozen Hartree-Fock method and coupling parameters taken from known nuclear structure data. Couplings to the  $3_1^-$  state in  $^{40}\text{Ca}$  and to the  $2_1^+$  states in  $^{58,64}\text{Ni}$  were included in the CC calculations. The resulting fusion barrier distributions were compared with experimental data as well as TDHF fusion thresholds which include automatically all types of couplings (inelastic and nucleon transfer channels) at the mean field level.

The lowering of the fusion threshold due to dynamical effects is explained in  $^{40}\text{Ca}+^{58}\text{Ni}$  without invoking trans-

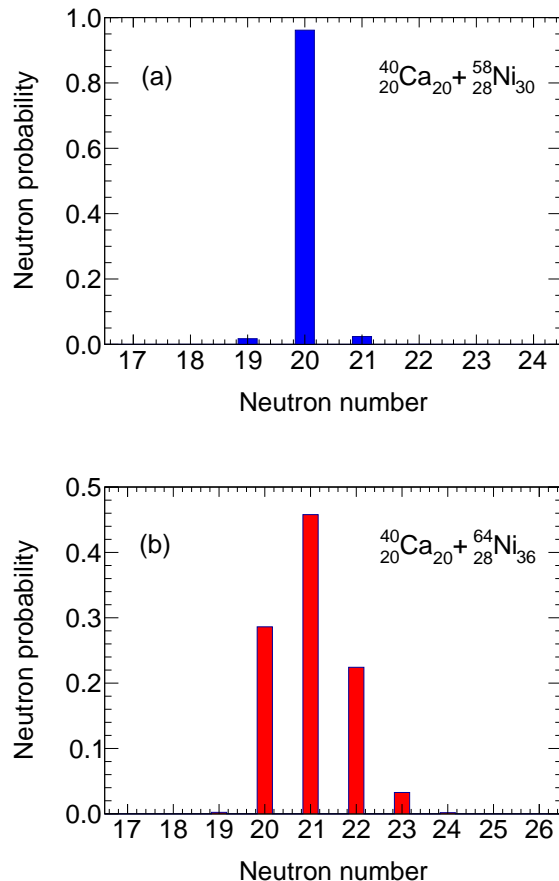


FIG. 4. (Color online) TDHF calculations of the Ca quasi-projectile neutron number distributions in the exit channel of (a)  $^{40}\text{Ca} + ^{58}\text{Ni}$  at  $E_{c.m.} = 71.65$  MeV and (b)  $^{40}\text{Ca} + ^{64}\text{Ni}$  at  $E_{c.m.} = 69.01$  MeV.

fer channels which are shown to be weak. The case of  $^{40}\text{Ca} + ^{64}\text{Ni}$  is different as inelastic couplings to low-lying phonons only account for about two third of the lowering of the fusion thresholds. Transfer channels which are shown to be important near barrier, could result in a further lowering of the fusion thresholds, possibly via neck formation.

Experimental measurement of nucleon transfer cross section around the fusion barrier for these two systems were recently performed to investigate directly this effect. It would also be interesting to extend the measurement of fusion cross sections at lower energies for these systems in order to better understand the role of transfer reactions on the deep sub-barrier fusion hindrance recently observed [84, 85].

Further theoretical investigations are also required to better understand the mechanisms of the couplings between transfer channels and fusion. In particular, transfer could favour neck formation and, thus, diffusion towards a compound nucleus. It has also been argued that transfer could be a doorway to dissipation hindering fusion [17].

## V. ACKNOWLEDGMENTS

The research leading to the experimental results mentioned in this paper has received funding from the European Commission within its Seventh Framework Programme under Grant Agreement No. 262010 ENSAR. This work has been supported by the Australian Research Council Grant No. FT120100760.

- 
- [1] J. R. Leigh *et al.*. Barrier distributions from the fusion of oxygen ions with  $^{144,148,154}\text{Sm}$  and  $^{186}\text{W}$ , Phys. Rev. C **52**, 3151 (1995).
  - [2] M. Dasgupta, D. J. Hinde, N. Rowley, and A. M. Stefanini. Measuring barriers to fusion, Ann. Rev. Nucl. Part. Sci. **48**, 401 (1998) and references therein.
  - [3] B. B. Back, H. Esbensen, C. L. Jiang, and K. E. Rehm. Recent developments in heavy-ion fusion reactions, Rev. Mod. Phys. **86**, 317 (2014) and references therein.
  - [4] C. H. Dasso, S. Landowne, and A. Winther. Channel-coupling effects in heavy-ion fusion reactions, Nucl. Phys. A **405**, 381 (1983).
  - [5] C. H. Dasso, S. Landowne, and A. Winther. A study of Q-value effects on barrier penetration, Nucl. Phys. A **407**, 221 (1983).
  - [6] R. Lindsay and N. Rowley. Approximate treatment of coupled-channels effects in sub-barrier fusion, J. Phys. G **10**, 805 (1984).
  - [7] I. J. Thompson, M. A. Nagarajan, J. S. Lilley, and B. R. Fulton. Contribution of multistep transfers to low-energy elastic and reaction cross sections, Phys. Lett. B **157**, 250 (1985).
  - [8] H. Esbensen and S. Landowne. Higher-order coupling effects in low energy heavy-ion fusion reactions, Phys. Rev. C **35**, 2090 (1987).
  - [9] A. M. Stefanini *et al.*. Elastic scattering of  $^{58}\text{Ni} + ^{64}\text{Ni}$  near the Coulomb barrier, Phys. Lett. B **240**, 306 (1990).
  - [10] A. B. Balantekin and N. Takigawa. Quantum tunneling in nuclear fusion, Rev. Mod. Phys. **70**, 77 (1998).
  - [11] K. Hagino and N. Takigawa. Subbarrier fusion reactions and many-particle quantum tunneling, Prog. Th. Phys. **128**, 1061 (2012).
  - [12] K. Washiyama and D. Lacroix. Energy dependence of the nucleus-nucleus potential close to the Coulomb barrier, Phys. Rev. C **78**, 024610 (2008).
  - [13] C. Simenel, R. Kesper, A. S. Umar, and V. E. Oberacker. Microscopic study of  $^{16}\text{O} + ^{16}\text{O}$  fusion, Phys. Rev. C **88**, 024617 (2013).
  - [14] C. Simenel, M. Dasgupta, D. J. Hinde, and E. Williams. Microscopic approach to coupled-channels effects on fu-

- sion, Phys. Rev. C **88**, 064604 (2013).
- [15] A. M. Stefanini, D. Ackermann, L. Corradi, J. H. He, G. Montagnoli, S. Beghini, F. Scarlassara, and G. F. Segato. Signatures of multiphonon and neutron transfer couplings in the fusion of  $^{36,32}\text{S}+^{110}\text{Pd}$ , Phys. Rev. C **52**, R1727(R) (1995).
  - [16] C. L. Jiang *et al.*. Fusion hindrance for Ca+Ca systems: influence of neutron excess, Phys. Rev. C **82**, 041601 (2010).
  - [17] M. Evers, M. Dasgupta, D. J. Hinde, D. H. Luong, R. Rafiei, R. du Rietz, and C. Simenel. Cluster transfer in the reaction  $^{16}\text{O}+^{208}\text{Pb}$  at energies well below the fusion barrier: a possible doorway to energy dissipation, Phys. Rev. C **84**, 054614 (2011).
  - [18] G. Montagnoli *et al.*. Effects of transfer channels on near- and sub-barrier fusion of  $^{32}\text{S}+^{48}\text{Ca}$ , Phys. Rev. C **87**, 014611 (2013).
  - [19] C. L. Jiang, K. E. Rehm, B. B. Back, H. Esbensen, R. V. F. Janssens, A. M. Stefanini, and G. Montagnoli. Influence of heavy-ion transfer on fusion reactions, Phys. Rev. C **89**, 051603 (2014).
  - [20] A. V. Karpov, V. A. Rachkov, and V. V. Samarin. Quantum coupled-channels model of nuclear fusion with a semiclassical consideration of neutron rearrangement, Phys. Rev. C **92**, 064603 (2015).
  - [21] C. Simenel and A. Benoit. Time-dependent Hartree-Fock description of heavy ions fusion, Int. J. Mod. Phys. E **17**, 31 (2008).
  - [22] A. S. Umar, V. E. Oberacker, and J. A. Maruhn. Neutron transfer dynamics and doorway to fusion in Time-Dependent Hartree-Fock theory, Eur. Phys. J. A **37**, 245 (2008).
  - [23] C. Simenel. Particle transfer reactions with the Time-Dependent Hartree-Fock theory using a particle number projection technique, Phys. Rev. Lett. **105**, 192701 (2010).
  - [24] K. Sekizawa and K. Yabana. Time-Dependent Hartree-Fock calculations for multinucleon transfer processes in  $^{40,48}\text{Ca}+^{124}\text{Sn}$ ,  $^{40}\text{Ca}+^{208}\text{Pb}$ , and  $^{58}\text{Ni}+^{208}\text{Pb}$  reactions, Phys. Rev. C **88**, 014614 (2013).
  - [25] K. Sekizawa and K. Yabana. Particle-number projection method in Time-Dependent Hartree-Fock theory: properties of reaction products, Phys. Rev. C **90**, 064614 (2014).
  - [26] J. B. Marston and S. E. Koonin. Mean-field calculations of fluctuations in nuclear collisions, Phys. Rev. Lett. **54**, 1139 (1985).
  - [27] P. Bonche and H. Flocard. Dispersion of one-body operators with the Balian-Vénéroni variational principle, Nucl. Phys. A **437**, 0375 (1985).
  - [28] C. Simenel. Particle-number fluctuations and correlations in transfer reactions obtained using the Balian-Vénéroni variational principle, Phys. Rev. Lett. **106**, 112502 (2011).
  - [29] K. Washiyama, S. Ayik, and D. Lacroix. Mass dispersion in transfer reactions with a stochastic mean-field theory, Phys. Rev. C **80**, 031602 (2009).
  - [30] B. Yilmaz, S. Ayik, D. Lacroix, and K. Washiyama. Nucleon exchange mechanism in heavy-ion collisions at near-barrier energies, Phys. Rev. C **83**, 064615 (2011).
  - [31] B. Yilmaz, S. Ayik, D. Lacroix, and O. Yilmaz. Nucleon exchange in heavy-ion collisions within a stochastic mean-field approach, Phys. Rev. C **90**, 024613 (2014).
  - [32] T. Skyrme. The nuclear surface, Phil. Mag. **1**, 1043 (1956).
  - [33] D. Vautherin and D. M. Brink. Hartree-Fock calculations with Skyrme's interaction. I. Spherical nuclei, Phys. Rev. C **5**, 626 (1972).
  - [34] D. Bourgin *et al.*. Barrier distributions and signatures of transfer channels in the  $^{40}\text{Ca}+^{58,64}\text{Ni}$  fusion reactions at energies around and below the Coulomb barrier, Phys. Rev. C **90**, 044610 (2014).
  - [35] K. Hagino, N. Rowley, and A. T. Kruppa. A Program for coupled-channel calculations with all order couplings for heavy-ion fusion reactions, Comput. Phys. Commun. **123**, 143 (1999).
  - [36] O. Akyüz and A. Winther. Nuclear surface-surface interaction in the folding model, in *Nuclear Structure and Heavy-Ion Physics*, Proc. Int. School of Physics "Enrico Fermi", Varenna, edited by R. A. Broglia and R. A. Ricci (North Holland, Amsterdam, 1981), p. 492.
  - [37] A. Winther. Dissipation, polarization and fluctuation in grazing heavy-ion collisions and the boundary to the chaotic regime, Nucl. Phys. A **594**, 203 (1995).
  - [38] K. -H. Kim, T. Otsuka, and P. Bonche. Three-dimensional TDHF calculations for reactions of unstable nuclei, J. Phys. G **23**, 1267 (1997).
  - [39] P. A. M. Dirac. Note on exchange phenomena in the Thomas atom, Proc. Camb. Phil. Soc. **26**, 376 (1930).
  - [40] P. A. M. Guichon, H. H. Matevosyan, N. Sandulescu, and A. W. Thomas. Physical origin of density dependent forces of Skyrme type within the quark meson coupling model, Nucl. Phys. A **772**, 1 (2006).
  - [41] M. Kortelainen, J. McDonnell, W. Nazarewicz, P. -G. Reinhard, J. Sarich, N. Schunck, M. V. Stoitsov, and S. M. Wild. Nuclear energy density optimization: large deformations, Phys. Rev. C **85**, 024304 (2012).
  - [42] J. W. Negele. The mean-field theory of nuclear structure and dynamics, Rev. Mod. Phys. **54**, 913 (1982).
  - [43] C. Simenel. Nuclear quantum many-body dynamics - from collective vibrations to heavy-ion collisions, Eur. Phys. J. A **48**, 152 (2012).
  - [44] A. S. Umar, M. R. Strayer, and P. -G. Reinhard. Resolution of the fusion window anomaly in heavy-ion collisions, Phys. Rev. Lett. **56**, 2793 (1986).
  - [45] C. Simenel, Ph. Chomaz, and G. de France. Quantum calculation of the dipole excitation in fusion reactions, Phys. Rev. Lett. **86**, 2971 (2001).
  - [46] A. S. Umar and V. E. Oberacker. Time-dependent response calculations of nuclear resonances, Phys. Rev. C **71**, 034314 (2005).
  - [47] J. A. Maruhn, P. G. Reinhard, P. D. Stevenson, J. Rikowska Stone, and M. R. Strayer. Dipole giant resonances in deformed heavy nuclei, Phys. Rev. C **71**, 064328 (2005).
  - [48] T. Nakatsukasa and K. Yabana. Linear response theory in the continuum for deformed nuclei: Green's function vs Time-Dependent Hartree-Fock with the absorbing boundary condition, Phys. Rev. C **71**, 024301 (2005).
  - [49] P. Bonche, B. Grammaticos, and S. Koonin. Three-dimensional Time-Dependent Hartree-Fock calculations of  $^{16}\text{O}+^{16}\text{O}$  and  $^{40}\text{Ca}+^{40}\text{Ca}$  fusion cross sections, Phys. Rev. C **17**, 1700 (1978).
  - [50] A. S. Umar, C. Simenel, and V. E. Oberacker. Energy dependence of potential barriers and its effect on fusion cross sections, Phys. Rev. C **89**, 034611 (2014).

- [51] V. E. Oberacker, A. S. Umar, J. A. Maruhn, and P. -G. Reinhard. Dynamic microscopic study of pre-equilibrium giant resonance excitation and fusion in the reactions  $^{132}\text{Sn}+^{48}\text{Ca}$  and  $^{124}\text{Sn}+^{40}\text{Ca}$ , *Phys. Rev. C* **85**, 034609 (2012).
- [52] C. Simenel, Ph. Chomaz, and G. de France. Quantum calculations of Coulomb reorientation for sub-barrier fusion, *Phys. Rev. Lett.* **93**, 102701 (2004).
- [53] L. Guo and T. Nakatsukasa. Time-Dependent Hartree-Fock studies of the dynamical fusion threshold, *EPJ Web of Conferences* **38**, 09003 (2012).
- [54] K. Washiyama. Microscopic analysis of fusion hindrance in heavy nuclear systems, *Phys. Rev. C* **91**, 064607 (2015).
- [55] A. S. Umar and V. E. Oberacker. Heavy-ion interaction potential deduced from Density-Constrained Time-Dependent Hartree-Fock calculation, *Phys. Rev. C* **74**, 021601 (2006).
- [56] J. Blocki and H. Flocard. Calculation of giant resonances with Time-Dependent Hartree-Fock, *Phys. Lett. B* **85**, 163 (1979).
- [57] Ph. Chomaz, Nguyen Van Giai, and S. Stringari. Lifetimes of monopole resonances in Time-Dependent Hartree-Fock theory, *Phys. Lett. B* **189**, 375 (1987).
- [58] C. Simenel and Ph. Chomaz. Nonlinear vibrations in nuclei, *Phys. Rev. C* **68**, 024302 (2003).
- [59] P. D. Stevenson, D. Almed, P. -G. Reinhard, and J. A. Maruhn. Monopole giant resonances and TDHF boundary conditions, *Nucl. Phys. A* **788**, 343c (2007).
- [60] B. Avez and C. Simenel. Structure and direct decay of giant monopole resonances, *Eur. Phys. J. A* **49**, 76 (2013).
- [61] P. Bonche, H. Flocard, and P. -H. Heenen. Solution of the Skyrme HF+BCS equation on a 3D mesh, *Comput. Phys. Commun.* **171**, 49 (2005).
- [62] K. Bennaceur, P. Bonche, and J. Meyer. Mean field theories and exotic nuclei, *C. R. Physique* **4**, 555 (2003).
- [63] J. Dobaczewski, M. V. Stoitsov, and W. Nazarewicz. Skyrme-HFB deformed nuclear mass table, ed. R. Bijker, R. F. Casten, and A. Frank, (AIP, New York, 2004), **726**, 51 (2004).
- [64] G. A. Lalazissis, S. Raman, and P. Ring. Ground-State properties of even-even nuclei in the relativistic mean-field theory, *At. Data Nucl. Data Tables* **71**, 1 (1999).
- [65] A. S. Umar and V. E. Oberacker. Dynamical deformation effects in sub-barrier fusion of  $^{64}\text{Ni}+^{132}\text{Sn}$ , *Phys. Rev. C* **74**, 061601 (2006).
- [66] K. Sekizawa and K. Yabana. Time-dependent Hartree-Fock calculations for multinucleon transfer and quasifission processes in  $^{64}\text{Ni}+^{238}\text{U}$  reaction, arXiv:1601.06656.
- [67] R. Bass, *Nuclear Reactions with Heavy Ions*, 1980, Springer-Verlag Berlin, Heidelberg.
- [68] K. Hagino, N. Takigawa, M. Dasgupta, D. J. Hinde, and J. R. Leigh. Adiabatic quantum tunneling in heavy-ion sub-barrier fusion, *Phys. Rev. Lett.* **79**, 2014 (1997).
- [69] A. M. Stefanini *et al.*. Influence of complex surface vibrations on the fusion of  $^{58}\text{Ni}+^{60}\text{Ni}$ , *Phys. Rev. Lett.* **74**, 864 (1995).
- [70] R. A. Broglia, C. H. Dasso, S. Landowne, and A. Winther. Possible effect of transfer reactions on heavy ion fusion at sub-barrier energies, *Phys. Rev. C* **27**, 2433 (1983).
- [71] D. Lehbertz *et al.*.  $^{12}\text{C}(^{16}\text{O}, \gamma)^{28}\text{Si}$  radiative capture: structural and statistical aspects of the  $\gamma$  decay, *Phys. Rev. C* **85**, 034333 (2012).
- [72] C. Simenel, D. J. Hinde, R. du Rietz, M. Dasgupta, M. Evers, C. J. Lin, D. H. Luong, and A. Wakhle. Influence of entrance-channel magicity and isospin on quasi-fission, *Phys. Lett. B* **710**, 607 (2012).
- [73] A. Wakhle, C. Simenel, D. J. Hinde, M. Dasgupta, M. Evers, D. H. Luong, R. du Rietz, and E. Williams. Interplay between quantum shells and orientation in quasifission, *Phys. Rev. Lett.* **113**, 182502 (2014).
- [74] V. E. Oberacker, A. S. Umar, and C. Simenel. Dissipative dynamics in quasifission, *Phys. Rev. C* **90**, 054605 (2014).
- [75] A. S. Umar, V. E. Oberacker, and C. Simenel. Shape evolution and collective dynamics of quasifission in the Time-Dependent Hartree-Fock approach, *Phys. Rev. C* **92**, 024621 (2015).
- [76] J. Toke *et al.*. Quasi-fission - the mass-drift mode in heavy-ion reactions, *Nucl. Phys. A* **440**, 327 (1985).
- [77] R. du Rietz, D. J. Hinde, M. Dasgupta, R. G. Thomas, L. R. Gasques, M. Evers, N. Lobanov, and A. Wakhle. Predominant time scales in fission processes in reactions of S, Ti and Ni with W: zeptosecond versus attosecond, *Phys. Rev. Lett.* **106**, 052701 (2011).
- [78] S. E. Koonin, K. T. R. Davies, V. Maruhn-Rezwani, H. Feldmeier, S. J. Krieger, and J. W. Negele. Time-Dependent Hartree-Fock calculations for  $^{16}\text{O}+^{16}\text{O}$  and  $^{40}\text{Ca}+^{40}\text{Ca}$  reactions, *Phys. Rev. C* **15**, 1359 (1977).
- [79] N. Rowley, G. R. Satchler, and P. H. Stelson. On the 'distribution of barriers' interpretation of heavy-ion fusion, *Phys. Lett. B* **254**, 25 (1991).
- [80] B. Avez, C. Simenel, and Ph. Chomaz. Pairing vibrations study with the Time-Dependent Hartree-Fock-Bogoliubov theory, *Phys. Rev. C* **78**, 044318 (2008).
- [81] G. Scamps and D. Lacroix. Effect of pairing on one- and two-nucleon transfer below the Coulomb barrier: a time-dependent microscopic description, *Phys. Rev. C* **87**, 014605 (2013).
- [82] W. von Oertzen and A. Vitturi. Pairing correlations of nucleons and multi-nucleon transfer between heavy nuclei, *Rep. Prog. Phys.* **64**, 1247 (2001).
- [83] D. Montanari *et al.*. Neutron pair transfer in  $^{60}\text{Ni}+^{116}\text{Sn}$  far below the Coulomb barrier *Phys. Rev. Lett.* **113**, 052501 (2014) and references therein.
- [84] C. L. Jiang *et al.*. Influence of nuclear structure on sub-barrier hindrance in Ni+Ni fusion, *Phys. Rev. Lett.* **93**, 012701 (2004).
- [85] M. Dasgupta, D. J. Hinde, A. Diaz-Torres, B. Bouriquet, Catherine I. Low, G. J. Milburn, and J. O. Newton. Beyond the coherent coupled channels description of nuclear fusion, *Phys. Rev. Lett.* **99**, 192701 (2007).